STRUCTURAL ANALYSIS OF DESIGNED TUBES UNDER AXIAL COMPRESSION: VARIATIONS OF APPLIED TEMPERATURE, MATERIAL TYPE, AND GEOMETRY DESIGN

Hensa Akbar Al Kautsar[1], Anandito Adam Pratama[1], Suryanto Suryanto[1], Aditya Rio Prabowo[1,*], Ristiyanto Adiputra[2], Heru Sukanto[1], Bambang Kusharjanta[1], Hermes Carvalho[3,4]

[1]Department of Mechanical Engineering, Sebelas Maret University, Surakarta, Indonesia
[2]Research Center for Hydrodynamics Technology, National Research and Innovation Agency (BRIN), Surabaya, Indonesia
[3]Department of Structural Engineering, Federal University of Minas Gerais, Minas Gerais, Brazil
[4]Department of Structural Engineering and Geotechnical, University of Sao Paulo, Sao Paulo, Brazil

*E-mail of corresponding author: aditya@ft.uns.ac.id

Aditya Rio Prabowo ⓘ 0000-0001-5217-5943,
Heru Sukanto ⓘ 0009-0008-3719-3607,
Hermes Carvalho ⓘ 0000-0002-4652-8068

Ristiyanto Adiputra ⓘ 0000-0003-3630-9432,
Bambang Kusharjanta ⓘ 0000-0002-0194-3268,

Resume

The research presented in this article consisted of analysis of the ship structural accidents at low temperatures and the effect of carbon percentage in various classifications of carbon steel, compared to the high tensile strength steel materials. The objective of this research was to fill the knowledge gap by expanding the understanding of the influence of low temperature, material, and structure on the axial compression test of tubes. The simulations as idealization of the compression test were conducted with variations in temperature, material carbon percentage, and geometry shape, using Finite Element Analysis (FEA). The results showed that at -100 °C, the material had the best ability to resist compression energy; high carbon steel had the highest strength at various carbon percentages, and the square geometry showed the best ability to absorb energy before failure.

Available online: https://doi.org/10.26552/com.C.2024.036

1   Introduction

Throughout history, people and goods have moved between continents and across oceans. Ocean transportation effectively and efficiently moves almost all goods across a wide range of expedition needs [1]. Ocean transportation is responsible for moving thousands of goods daily, contributing to global trade [2]. Media and scientists predict that an increase in ship traffic will occur [3]. Results introduced by scholars in [4-5] indicate that the consequences of large volumes of global ocean transportation are also associated with negative environmental impacts on the marine environment. In pioneer researaches, such as [6-7], it is also stated that accidents at sea pose significant risks to individuals and society in various fields, and ship collisions are one of the main contributors to frequent maritime traffic accidents. Figure 1 shows the high frequency and severe consequences of collisions, both practitioners and researchers have paid attention to related research, and various types of techniques aimed at preventing accidents and reducing the risks resulting from accidents have been developed [8-11].

For the safety of ship structures, predicting the load-carrying capacity of these types of members is crucial. There are several methods to estimate the collapse behavior of ship structures, including experiments, numerical analysis, analytical methods, and so on [13-15]. Huhne et al. [16] conducted 4000 tests; the test results and numerical analysis showed that the approach used has the potential to provide better and less conservative designs. This approach is used in designs that show that imperfect buckling loads must be maximized to determine a realistic optimal
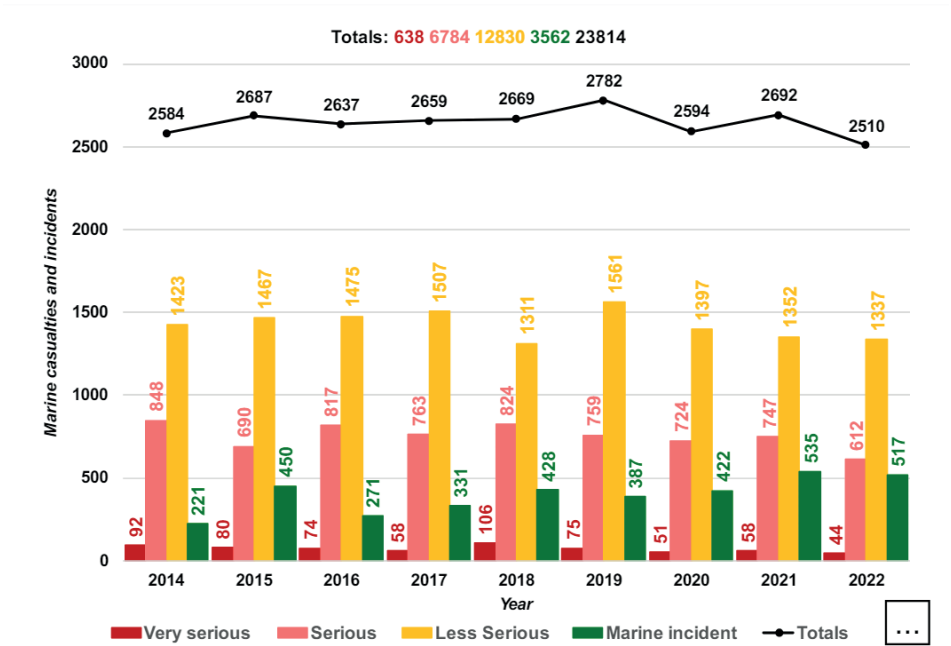
Totals: 638 6784 12830 3562 23814

Figure 1 *Number of marine casualties and incidents [12]*

Table 1 *Material parameters of the mild steel*

Parameter	Notation, unit	Mild Steel
Density	ρ (kg/m^3)	7850
Modulus of elasticity	E (N/m^2)	203 x 10^9
Poisson's ratio	v	0.33
Johnson-Cook flow stress parameters		
Initial yield stress	A (N/m^2)	304.33 x 10^6
Hardening coefficient	B (N/m^2)	422 x 10^6
Hardening exponent	n	0.345
Strain rate constant	C	0.0156
Thermal softening constant	m	0.87
Reference strain rate	$\dot{\varepsilon}_0 \left(s^{-1} \right)$	0.0001
Melting temperature	T_{melt} (K)	1800
Transition temperature	T_0 (K)	293
Johnson-Cook fracture strain parameters		
Fracture strain constant	D_1	0.1152
	D_2	1.0116
	D_3	- 1.7684
	D_4	- 0.05279
	D_5	0.5262

design. Another study, conducted by McGregor et al. [17], showed the success of modelling in numerical simulation helps in the achievement of good design for future integration of composites into collision-resistant structures, good calculations contribute to the design objectives of the parts safely and efficiently for final integration into collision structures. Another study, was presented by Greiner et al. [18], which discussed the interaction of bending and axial compression. The study results showed that the interaction behavior of stainless steel under the load can be represented by interaction testing of the same structure as for carbon steel. The study conducted in [18] covers a wide range of practical sections. However, a number of other parameters have not been investigated, which suggests that further research is needed to compare the interaction behavior of carbon steel to other types of steel. In axial compression testing, low-carbon steels tend to have lower strength
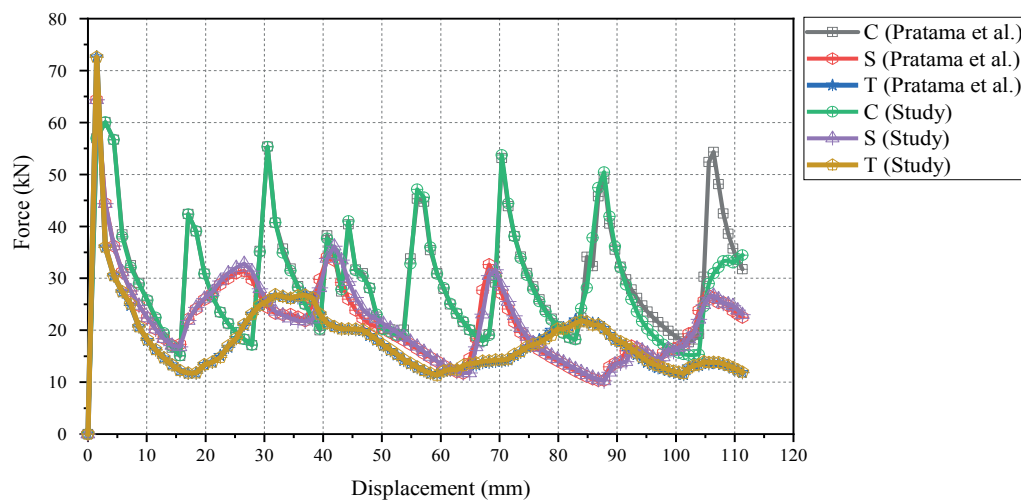
Figure 2 Force-Displacement comparison diagram to Pratama et al. [24]; C = Cylinder, S = Square, and T = Triangle

Table 2 Error percentage comparison to research of Pratama et al. [24]

| Output	Geometry	Pratama et al. [24]	Current Study	Error (%)
Maximum Displacement (mm)	Cylinder	90.53	91.00	0.519165
	Square	103.54	103.14	0.386324
	Triangle	111.39	111.32	0.062842
Total Energy Absorption (J)	Cylinder	2707.64	2665.86	1.543041
	Square	2271.06	2285.92	0.65432
	Triangle	2031.69	2036.89	0.255945
Peak Force (kN)	Cylinder	60.09	60.10	0.016642
	Square	64.40	64.40	0
	Triangle	72.62	72.58	0.055081
Average Force (kN)	Cylinder	29.66	28.48	3.978422
	Square	21.10	21.29	0.900474
	Triangle	17.62	17.68	0.340522
Average				0.726
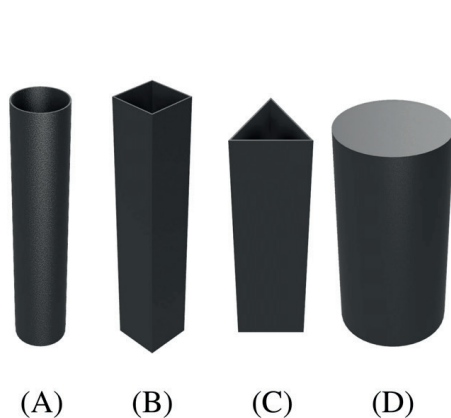
Figure 3 Geometrical design; (A) Cylindrical Tube, (B) Square Tube, (C) Triangular Tube, and (D) Impactor
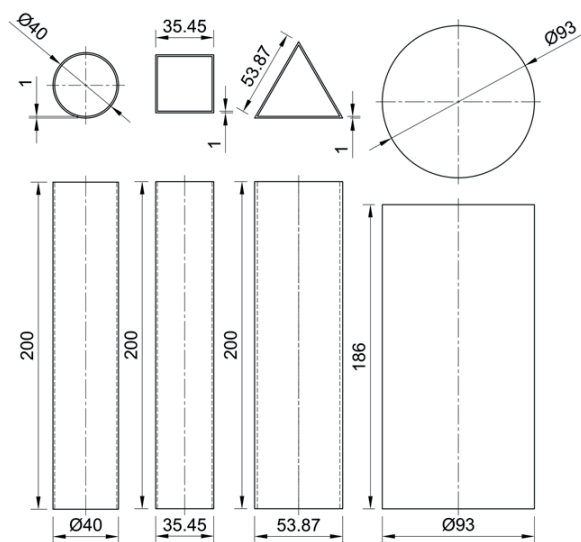

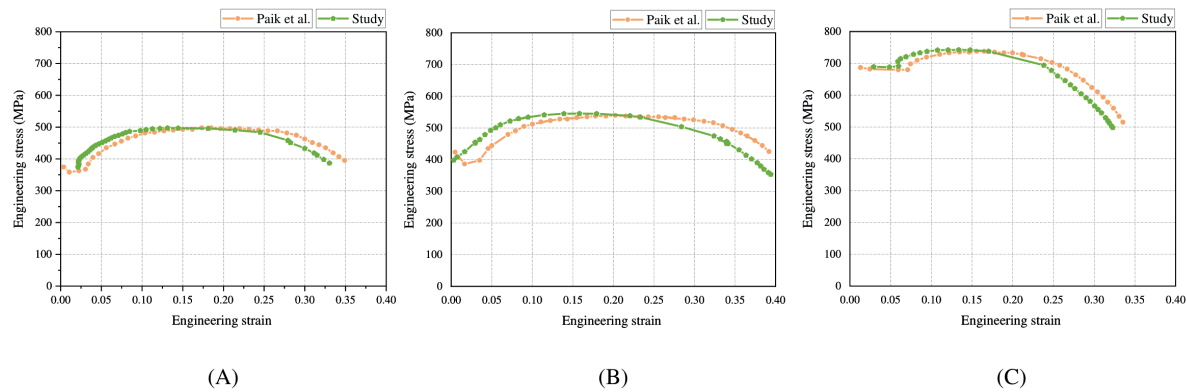*Figure 4* Dimensions of geometrical design; in (mm)

Figure 5 *Comparison of engineering stress-strain curve to results introduced by Paik et al. [19]; (A) at 20 °C, (B) at -40 °C, and (C) at -160 °C*

Table 3 *Variation of the AH32 input parameters at low temperature [19]*

Property	Temperature (°C)					
	20	-40	-80	-100	-130	-160
Yield strength, σ_y (MPa)	359.65	369.06	381.01	386.22	387.20	411.51
Fracture strain, ε_{ft}	0.376	0.423	0.430	0.448	0.409	0.336

Table 4 *Material parameter of used steels ASTM A36 [31-33]; AISI 1045 [34-36] and AISI 52100 [34, 36]*

Parameter	Notation	ASTM A36	AISI 1045	AISI 52100
Density	ρ (kg/m³)	7850	7850	7810
Modulus of elasticity	E (N/m²)	200 x 10⁹	205 x 10⁹	200 x 10⁹
Poisson's ratio	v	0.26	0.29	0.3
Johnson-Cook flow stress parameters				
Initial yield stress	A (N/m²)	250 x 10⁶	506 x 10⁶	774.48 x 10⁶
Hardening coefficient	B (N/m²)	477 x 10⁶	320 x 10⁶	134 x 10⁶
Hardening exponent	n	0.18	0.28	0.37
Strain rate constant	C	0.012	0.064	0.018
Thermal softening constant	m	1	1.06	3.171
Reference strain rate	$\dot{\varepsilon}_0\,(s^{-1})$	0.0001	0.0001	0.0001
Melting temperature	T_{melt} (K)	1811	1733	1424
Transition temperature	T_0 (K)	300	300	300
Johnson-Cook fracture strain parameters				
Fracture strain constant	D_1	0.403	0.1	0.0368
	D_2	1.107	0.76	2.34
	D_3	- 1.899	- 1.57	- 1.484
	D_4	0.00961	0.005	0.0035
	D_5	0.3	-0.84	0.411

with good ductility; medium-carbon steels balance the strength and ductility, while the high-carbon steels have high strength but may lack ductility. Paik et al. in 2020 conducted tests experimentally for ship structural requirements, the test database developed in this study can be used to validate computational models for structural accident analysis under low temperature conditions, [19]. The researchers recommended further studies in computational models for structural accident analysis at low temperatures, since then the high tensile

strength steel materials tend to decrease in strength and elastic modulus, which can affect the increase in material stress at low temperatures. At low temperatures, ship structures need to be designed, taking into account the material's potential fragility, dimensional changes, and the need for thermal insulation to ensure optimal safety and performance.

The Northern Sea Route (NSR) is one of the sea trade routes connecting Asia and Europe. According to studies, for examples [20-21], the NSR cuts emissions, fuel consumption by around 40 %, and shipping distances. The location is unsuitable for maritime transit due to the exceptionally low temperatures, which also pose a hazard to ships [22-23]. Consequently, a more thorough analysis of ship structural mishaps at low temperatures is required. The impact of low temperatures on the strength of materials suitable for use in ship structures is explored in this study. Furthermore, the authors delft into the impact of carbon percentage on every carbon steel classification, drawing comparisons to high tensile strength steel material.

In the available literature, there is limited research on the effect of low temperature, material, and structure on the axial compression test of tubes. So far, several studies have focused on the effect of low temperature but on tensile testing, as well as studies focusing on axial compression tests but with different test variations such as corrosion and test angle. Therefore, there is still a significant lack of information on the reaction of tubes when exposed to axial compression loads. Thus, the objective of this research was to fill the testing gap by expanding the understanding of the effect of temperature, material composition, and geometry on the strength of a structure.

2 Benchmark particulars

2.1 Model references

Before conducting research using numerical analysis, it is necessary to conduct methodology verification to ensure the fidelity of the deployed numerical method. Therefore, benchmark analysis is performed with an objective to obtain numerical method that results similar output compared to the benchmark reference. In this study, numerical model was built by adopting same methodology as in the reference, i.e., model size, FEA configuration, and loading conditions. The research geometry variation was equalized with the study conducted in [24], namely cylinder of a diameter of 40 mm, square of a length of each side of 35.45 mm, and triangle of a length of each side of 53.87 mm, each tube has the same height of 200 mm, using the direction of the impactor load angle adjusted to 0 ° as an illustration of deformation caused by ship collisions. The use of a mesh was also adjusted to a value of 1 mm. Table 1 shows that in this study were used the material parameters adapted

to [24], as well. The research aim was to comprehend how the mild steel materials, which are frequently used in shipbuilding, behave when subjected to compression. The computational methods were employed to investigate thin-walled metal tubes response to static and dynamic loads. The three-dimensional computational models were used to examine the thin-walled metal tubes with varying sizes and forms, under the static and dynamic loads. The ABAQUS software was employed to create the model, and the impact response of the tube was examined in terms of its diameter and form. Simulations were run to comprehend the tube's deformation and energy absorption under varied load situations. The research method was carried out using the design of empty tube structure, validation of the numerical method, variation of tube design, and explicit dynamic simulation. The parametric study was conducted by varying the geometric shape of the tube, load angle, and corrosion location to understand the axial deformation and energy absorption. Results showed that round tubes had the best resistance.

The Johnson-Cook model [25] can be used to characterize the material of the model to be used in the simulation. In this model the material flow is made as a combination of the linear thermo-elasticity, von Mises yield criterion, isotropic strain hardening, strain rate hardening, and softening due to adiabatic effects. The equivalent von Mises stress σ of the Johnson-Cook model is expressed as:

$$\bar{\sigma}(\bar{\varepsilon}^{pl}, \dot{\bar{\varepsilon}}^{pl}, \hat{T}) = \left[A + B(\bar{\varepsilon}^{pl})^n \right] \left[1 + C \ln\left(\frac{\dot{\bar{\varepsilon}}^{pl}}{\dot{\varepsilon}_0}\right) \right] \cdot \\ \cdot [1 - \hat{T}^m], \tag{1}$$

where, A, B, n, C and m are material parameters obtained from various tensile tests. $\dot{\varepsilon}_0$ is the reference strain rate, $\bar{\varepsilon}^{pl}$ is equivalent plastic strain, $\dot{\bar{\varepsilon}}^{pl}$ is equivalent to plastic strain rate, and $\hat{T}$ is dimensionless parameter. The equivalent fracture strain in the Johnson-Cook model is given as:

$$\bar{\varepsilon}_f^{pl}\left(\frac{\sigma_m}{\bar{\sigma}}, \dot{\bar{\varepsilon}}^{pl}, \hat{T}\right) = \left[D_1 + D_2 \exp\left(D_3 \frac{\sigma_m}{\bar{\sigma}}\right) \right] \cdot \\ \left[1 + D_4 \ln\left(\frac{\dot{\bar{\varepsilon}}^{pl}}{\dot{\varepsilon}_0}\right) \right] [1 + D_5 \hat{T}], \tag{2}$$

where D_1, D_2, and D_3 represent the stress triaxiality parameters, D_4 is the parameter of strain rate-dependent damage, D_5 is temperature-dependent fracture strain parameter, $\frac{\sigma_m}{\bar{\sigma}}$ is the stress triaxiality ratio, σ_m is the mean stress, and $\bar{\sigma}$ is the equivalent von Mises stress.

2.2 Benchmark results

As validation was needed in this research, the results conducted by [24] on the output of maximum displacement, peak force, average force, and total energy

absorption, were compared. The result comparisons, as a validation step, are shown in Figure 2 where the comparison of the Force-Displacement diagram had conformity with the reference, and Table 2 shows a comparison of output values with an average percentage error of 0.72 %.

3 Methodology

3.1 Geometrical model

In this numerical analysis-based research, the component design consists of two parts, namely the tube and the impactor. Shown in Figures 3 and 4, the tube used had three geometry variations: Cylinder, Square, and Triangle, with their respective dimensions, equated with those of reference. In this research, the three geometries used the same material properties; the variation was conducted to analyze the effect of tube geometry on material strength. The impactor is defined as a rigid object that would not deform.

3.2 Applied material

3.2.1 Low variations

In this study, validation of applied material in numerical analysis with previous testing was also carried out by comparing the output of the last experimental testing results to production of the results in the numerical analysis corresponding to this test. Specifically, as shown in Figure 5, a comparison was made between the Engineering Stress-Strain output of the experimental test conducted in study by Paik et al. [19] and the output obtained from this numerical analysis. Comparisons were made between several tests since they were considered representative of the numerical analysis results. Temperature variations were performed on the AH32 Steel material by adjusting the experimental testing of reference, namely 20 °C, -40 °C, -80 °C, -100 °C, -130 °C, and -160 °C. Table 3 shows that for each temperature variation performed, the difference in parameter input is adjusted to experimental testing, as well, namely in the yield strength and fracture strain.

3.2.2 Carbon steel classifications

The American Iron and Steel Institute (AISI) defines carbon steel as a steel that has no specified minimum content or requirements for chromium, cobalt, niobium, molybdenum, nickel, titanium, tungsten, vanadium, or zirconium, or special requirements for other elements. The low-carbon steel contains up to 0.30 % carbon; it has high formability due to its shallow carbon content. The medium carbon steels are similar to low carbon

steels except that they contain from 0.30 % to 0.60 % carbon, and the increase in carbon content allows medium carbon steels to be used in quenched and tempered conditions. The high-carbon steel contains carbon from 0.60 % to 1.00 %; it is used for some hand tools, spring materials, high-strength wires, etc. The high-strength low-alloyed (HSLA) is a micro-alloyed steel designed to improve mechanical properties. It may also have more excellent resistance to atmospheric corrosion and low temperatures than the conventional carbon steels. The HSLA steels have low carbon content (0.05 % - 0.25 %) to produce adequate formability and weldability [26].

In this study, the ASTM A36 steel was used as the applied material in the low-carbon steel classification, because it has a carbon content of 0.25 %, as stated by [27]. The AISI 1045 steel is in the medium carbon steel classification because it has a carbon content of around 0.312 %, as stated by [28]. The AISI 52100 steel is in the high carbon steel classification because it has a carbon content of around 0.95 %, as [29] stated. The AH32 steel is in the HSLA steel classification because it has material characteristics by this classification and has a carbon content of around 0.12 %, as stated by [30]. Table 4 shows the used material parameters.

3.3 Finite element setting

In this study, the placement and setting of boundary conditions were critical to ensure the reproduction of physical test conditions, prevent unwanted wave reflections, maintain the numerical stability, enable correlation with experimental data, and support structural design optimization. Displacement/rotation and encastre boundary conditions were the boundary conditions used. Encastre boundary conditions were placed on the side of the hollow tube that had no contact with the impactor. Displacement/rotation boundary conditions were placed on the side of the tube that contacted with the impactor. Figure 6 shows the boundary condition setup. The loading is carried out using an impactor in an axial direction towards the tube.

The mesh arrangement in the hollow tube model uses the S4R shell element settings in the ABAQUS software. The mesh used in the simulation is 1 mm. As presented in Figure 7, the first and second major peaks are shown in the convergence study a starting from mesh size 2.5 mm and larger, which is noted by the limit line. Based on stability criteria for the mesh convergence, i.e., (1) the fluctuation between two closest mesh sizes is less than 10%, and (2) no rise or decline on the results more than one mesh size; it can be concluded that the recommended mesh sizes are in the range of 0 - 2.5 mm. The indication of the recommended mesh is highlighted by red lines in Figure 7.

The displacement/rotation boundary condition restricts the movement of the selected degrees of
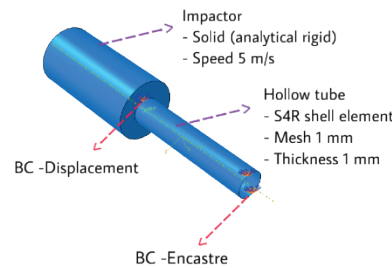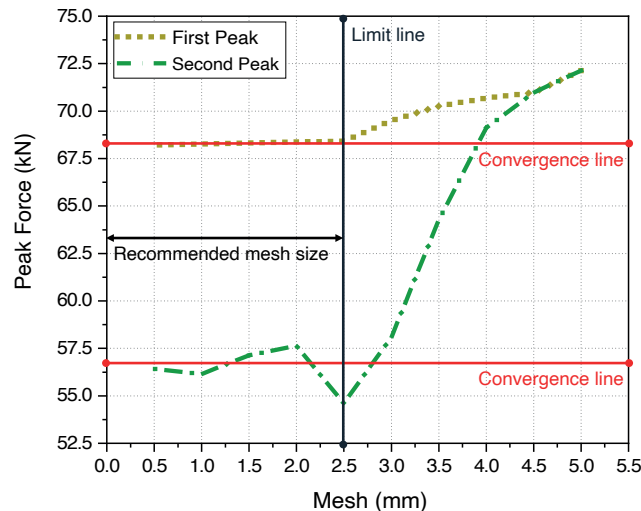
Figure 6 Boundary conditions setting

Figure 7 Mesh convergence diagram

Table 5 Scenario of simulations

Material	Temperature (°C)	Geometrical
Low carbon (ASTM A36)	20	Cylinder, square, and triangle
Medium carbon (AISI 1045)	20	Cylinder, square, and triangle
High carbon (AISI 52100)	20	Cylinder, square, and triangle
HSLA (AH32)	20	Cylinder, square, and triangle
	-40	Cylinder, square, and triangle
	-80	Cylinder, square, and triangle
	-100	Cylinder, square, and triangle
	-130	Cylinder, square, and triangle
	-160	Cylinder, square, and triangle

freedom. The degrees of freedom are in the Y-axis direction and parallel to the impact axis direction. The encase boundary condition allows structural degrees of freedom on the side of the tube without contact with the impactor to be considered fixed. The interaction between the tube and the impactor is constrained and coupled at one geometric point. The contact between the impactor and the tube is modelled with a friction coefficient of 0.05, as shown by previous research conducted in [37]. The impact velocity was set with a constant velocity value of 5 m/s since in [38] was mentioned that ship collisions can be assumed with this value. Table 5 shows the finite element simulation variations were conducted on tube geometry, temperature, and material.

4   Results and discussion

The content of this research discusses the effect of different shapes and material compositions on axial compression testing as a numerical analysis intended as a ship structure material. The research is also intended to determine the effect of temperature on the material. The output of numerical analysis results in the form of maximum displacement, total energy absorption, peak

Table 6 *Finite element simulation output with temperature variations; C = Cylinder, S = Square, T = Triangle, and Av = Average*

Temp. (°C)	Maximum displacement (mm)				Total energy absorption (J)			
	C	S	T	Av	C	S	T	Av
20	84.10	97.33	92.16	91.20	2731.89	2394.67	2582.49	2569.68
-40	82.79	98.49	93.55	91.61	2799.91	2382.42	2545.22	2575.85
-80	81.11	97.35	92.97	90.48	2798.40	2399.74	2567.45	2588.53
-100	82.08	97.33	86.81	88.74	2785.68	2413.91	2642.51	2614.03
-130	82.61	96.98	87.08	88.89	2776.13	2404.35	2586.82	2589.10
-160	79.73	94.94	87.14	87.27	2826.91	2455.39	2658.75	2647.01
Av	82.07	97.07	89.95		2786.49	2408.41	2597.21	
Temp. (°C)	Peak force (kN)				Average force (kN)			
	C	S	T	Av	C	S	T	Av
20	68.27	73.36	85.03	75.55	31.37	23.03	26.93	27.11
-40	69.65	74.85	86.85	77.17	32.67	22.93	26.04	27.21
-80	71.56	76.89	89.37	79.27	33.45	23.21	26.54	27.73
-100	72.18	77.55	90.18	79.97	32.65	23.36	28.33	28.11
-130	72.32	77.71	90.37	80.13	32.29	23.30	27.41	27.67
-160	75.88	81.57	95.09	84.18	33.99	24.09	29.14	29.07
Av	71.64	76.99	89.48		32.74	23.32	27.40	

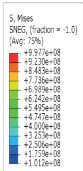**Table 7** *Tube deformation contour of cylindrical geometry at several temperatures*
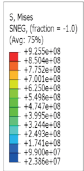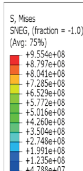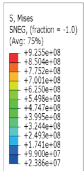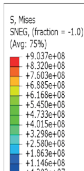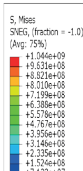
Temp. (°C)	Cylinder Geometry	Temp. (°C)	Cylinder Geometry
20		-100	
-40		-130	
-80		-160	

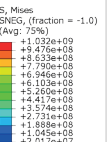**Table 8** *Tube deformation contour of square geometry at several temperatures*
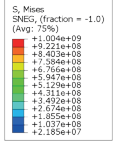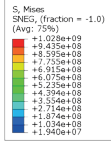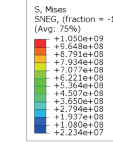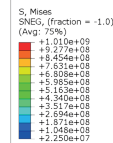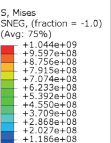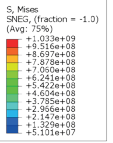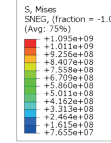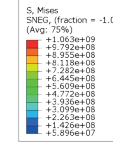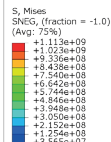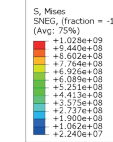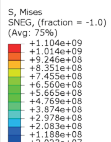
Temp. (°C)	Square Geometry	Temp. (°C)	Square Geometry
20		-100	
-40		-130	
-80		-160	

Table 9 *Tube deformation contour of triangle geometry at several temperatures*

Temp. (°C)	Triangle Geometry	Temp. (°C)	Triangle Geometry
20		-100	
-40		-130	
-80		-160	

Cylinder

Square

Triangle

Figure 8 *Force-displacement diagram of finite element simulation results with temperature and geometry variations*

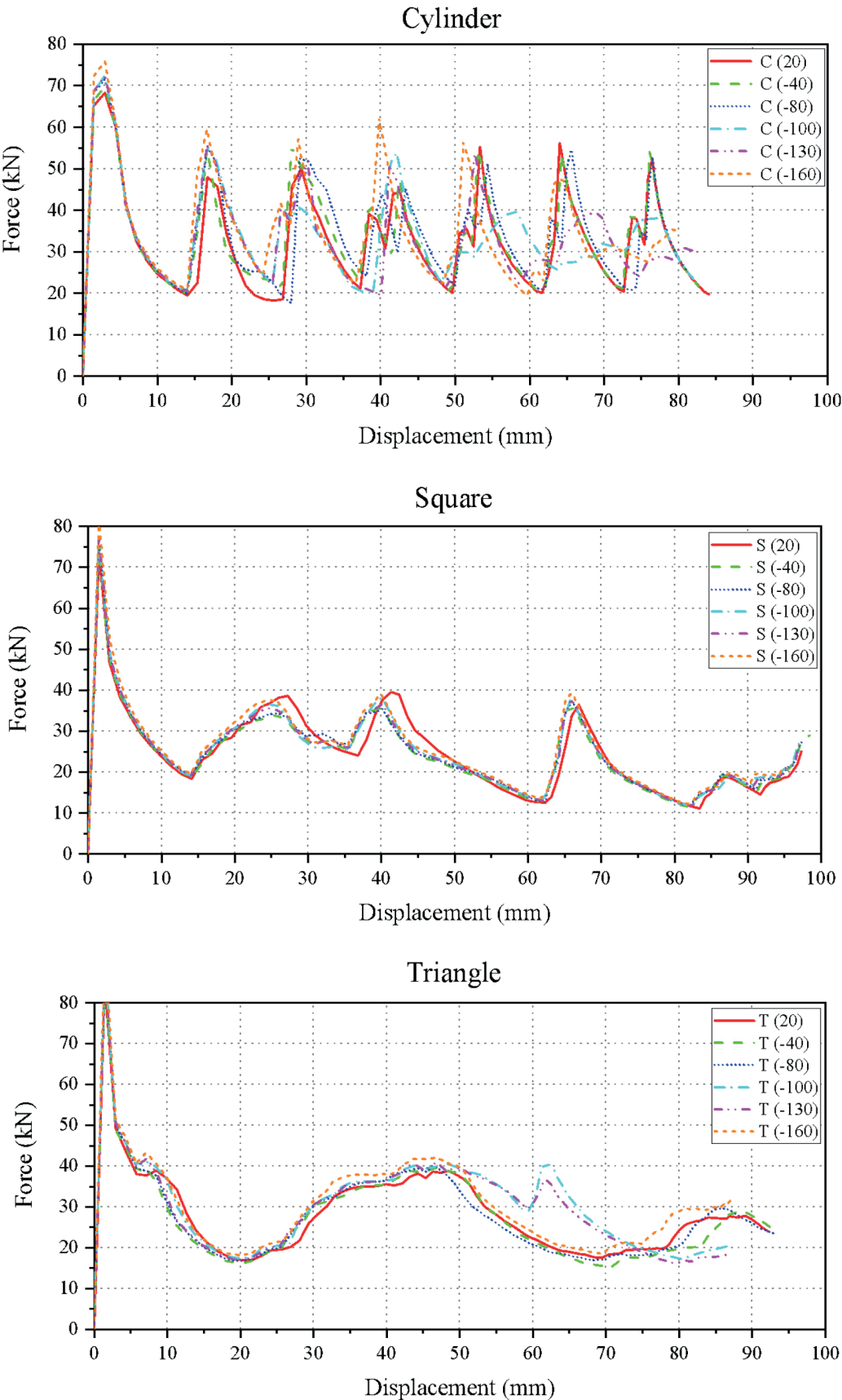**Table 10** *Finite element simulation output with carbon content variations; C = Cylinder, S = Square, T = Triangle, and Av = Average*

Class	Maximum displacement (mm)				Total energy absorption (J)			
	C	S	T	Av	C	S	T	Av
HSLA	84.10	97.33	92.16	91.20	2731.89	2394.67	2582.49	2569.68
Low	81.60	90.50	103.02	91.71	2782.38	2597.08	2354.95	2578.14
Medium	55.56	67.64	80.29	67.83	2824.38	2823.34	2722.20	2789.97
High	44.49	46.16	62.39	51.01	2818.60	2772.72	2785.53	2792.28
Av	66.44	75.41	84.46		2789.31	2646.95	2611.29	
Class	Peak force (kN)				Average force (kN)			
	C	S	T	Av	C	S	T	Av
HSLA	68.27	73.36	85.03	75.55	31.37	23.03	26.93	27.11
Low	70.98	74.12	83.89	76.33	32.67	26.97	22.20	27.28
Medium	91.44	100.01	114.08	101.84	37.48	38.41	31.61	35.83
High	120.21	135.78	153.24	136.41	37.73	38.08	38.59	38.13
Av	87.72	95.82	109.06		34.81	31.62	29.83	
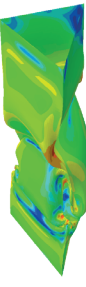
Table 11 *Tube deformation contour of cylinder geometry at material types*

Material Type	Cylinder Geometry
HSLA	
Low-carbon	
Medium-carbon	
High-carbon	
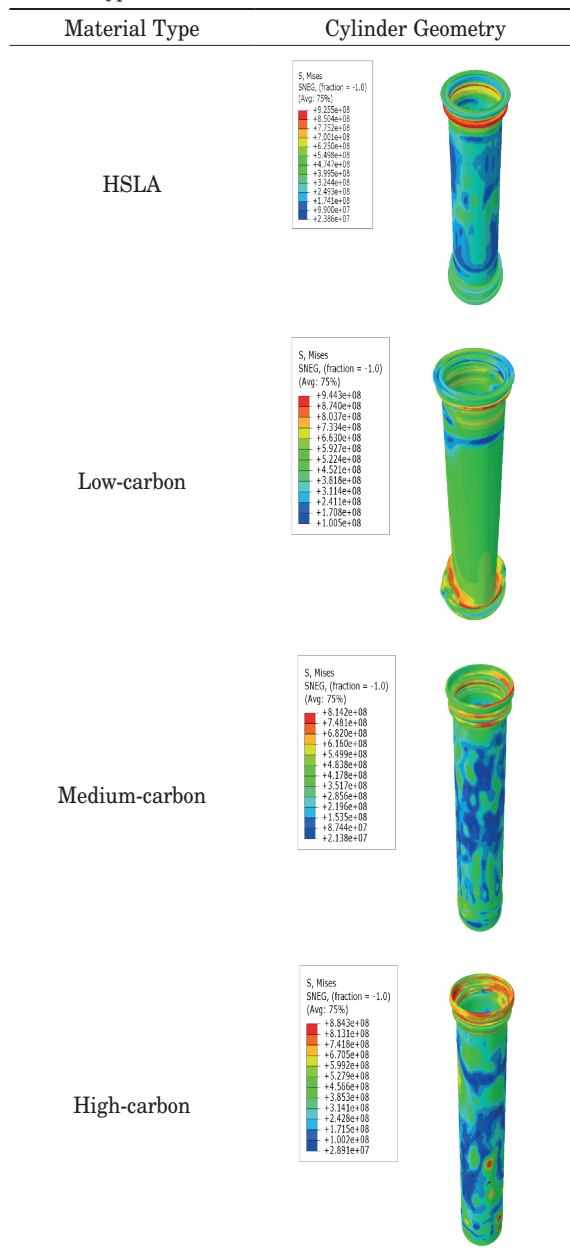
Table 12 *Tube deformation contour of square geometry at material types*

Material Type	Square Geometry
HSLA	
Low-carbon	
Medium-carbon	
High-carbon	
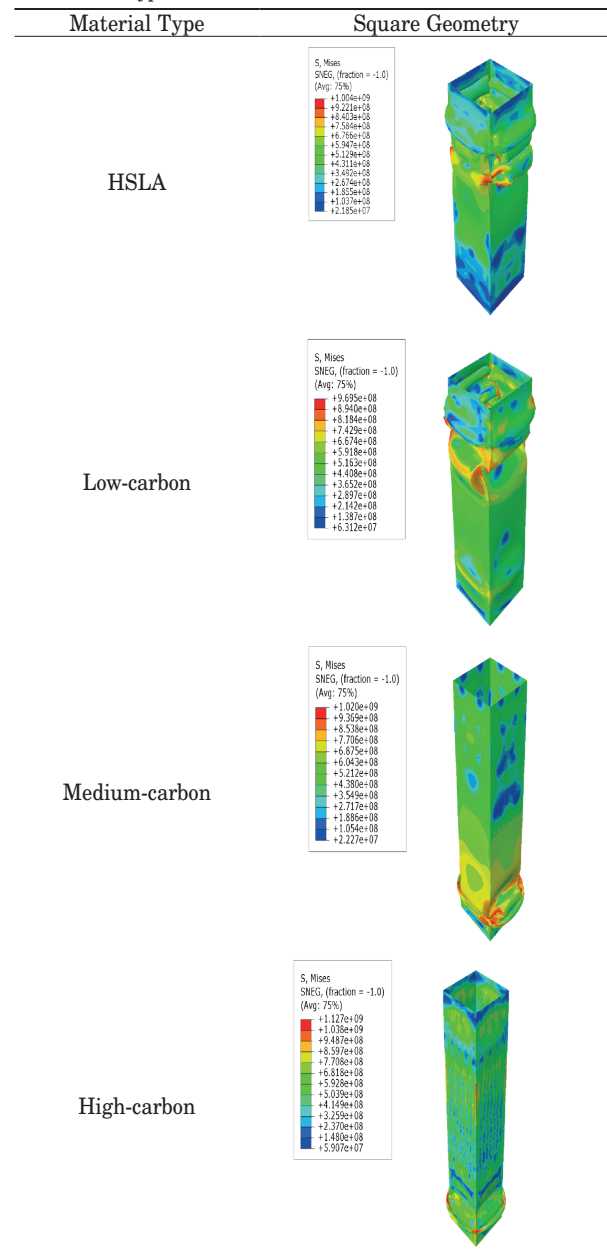
Table 13 *Tube deformation contour of triangle geometry at material types*

Material Type	Triangle Geometry
HSLA	
Low-carbon	
Medium-carbon	
High-carbon	

force, and average force are obtained in each simulation variation performed.

4.1 The effect of low temperatures

In this numerical analysis, the material selected in the test with low temperature variation was AH32 steel, because such is considered in accordance with previous study conducted by Suryanto et al. [39]. The numerical simulation was varied by inputting different material characteristics according to the material characteristics when subjected to temperatures of 20 °C, -40 °C, -80 °C, -100 °C, -130 °C, and -160 °C. This test was also validated on different geometries. As shown in Figure 8, it is found that at -100 °C, there are the most peaks and valleys in the force-displacement graph, which can be interpreted that the material can withstand greater compression energy at that temperature. Table 6 shows the output of the finite element simulation results,

where at Maximum Displacement the highest value was at -40 °C namely 91.61 mm, which indicates that at that temperature the specimen can absorb more energy before reaching the failure point. The Total Energy Absorption had the highest value at -160 °C namely 2647.01 J, indicating that at that temperature the material had good resistance to deformation and failure. The Peak Force highest value was at -160 °C namely 84.18 kN, which indicates that at that temperature the material had good strength and can withstand significant external loads before failure. The Average Force highest value was at -160 °C namely 29.07 kN, which indicates that at that temperature the material underwent consistent deformation. Table 7 to 9 shows a comparison of the final deformation contour shape of the tube with temperature variations.

4.2 The effect of carbon content

In this research, the materials used in the finite element simulation were ASTM AH32 in HSLA classification, ASTM A36 in low carbon steel classification, AISI 1045 in medium carbon steel classification, and 52100 in high carbon steel. The simulation was also validated using several geometries. Figure 9 shows that it was found that the HSLA steel had the most peaks and valleys in the force-displacement graph, which can be interpreted that at that temperature the material is able to withstand greater compression energy. In Table 10, one can see the output of the simulation results, where the highest Maximum Displacement value was found in the low carbon steel, namely 91.71 mm, indicating that the simulation specimen was able to absorb more energy before reaching the failure point. The highest Total Energy Absorption value was found in the high carbon steel, namely 2792.28 J, indicating that the material had good resistance to deformation and failure. The highest Peak Force value was found in the high carbon steel, namely 136.41 kN, indicating that the material had good strength and can withstand significant external loads before failure, and the highest Average Force value was found in the high carbon steel 38.13 kN, indicating that the material underwent consistent deformation. Tables 11 to 13 shows a comparison of the final deformation contour shape of the tube with temperature variations.

4.3 The effect of geometry

In this research, the geometries used in the numerical simulation were cylinder, square, and triangle. Figures 8 and 9 show that the cylinder geometry had the most peaks and valleys on the force-displacement graph, which can be interpreted that at that temperature the material can withstand greater compression energy. Table 14 shows the output of the numerical simulation

results, where in Maximum Displacement the highest value was in Triangle geometry, namely 87.2 mm, which indicates that in that geometry the simulation object was able to absorb more energy before reaching the point of failure. The Total Energy Absorption highest value was in Cylinder geometry, namely 2787.9 J, which indicates that in that geometry the material had good resistance to deformation and failure. The highest Peak Force value was found in the Triangle geometry namely 99.27 kN, which indicated that in that geometry the material had good strength and can withstand significant external loads before failure, and the highest Average Force value was found in the Cylinder geometry, namely 33.77 kN, which indicates that in that geometry the material was consistently deformed. Tables 7 and 9 show the comparison of the contour shape of the final deformation of the tube with geometry variations.

5 Conclusions

In this research, the authors examined the impact of low temperature and carbon percentage, validated by geometry variation, on the strength of materials used in ship structures, focusing on numerical idealization and analysis of axial compression testing. Then, investigations were conducted using a numerical approach to understand how low temperature, carbon percentage variation, and geometry shape affect the material's response to axial compression. Based on this understanding, this study could contribute to development of knowledge about material behaviour and helps to formulate safer and more efficient design strategies for future ship structures.

The results of this study using a numerical approach through ABAQUS software found that overall, in terms of the effect of low temperature effects, the displacement value decreases with decreasing temperature. In these terms, it means that the lower the temperature or the closer to the low temperature (-160 °C) will cause an increase in the strength of the material used. On the other hand, this results in an insignificant increase in total energy absorption, peak force, and average force. Then, regarding the effect of the percentage of carbon content, the HSLA-type material is the least strong. This is indicated by the many peaks and valleys produced in the force-displacement graph. Meanwhile, the more robust materials are high, medium, and low-carbon steels. In addition, the effect of the compression numerical specimen's geometric shape was also examined in this study. The square shape was the least strong because it experienced the most considerable deformation, followed by the triangular and cylindrical shapes.

This study has limitations related to the simplified representation of the mathematical model and factors that may occur in actual experimental testing, such as temperature changes during the testing process
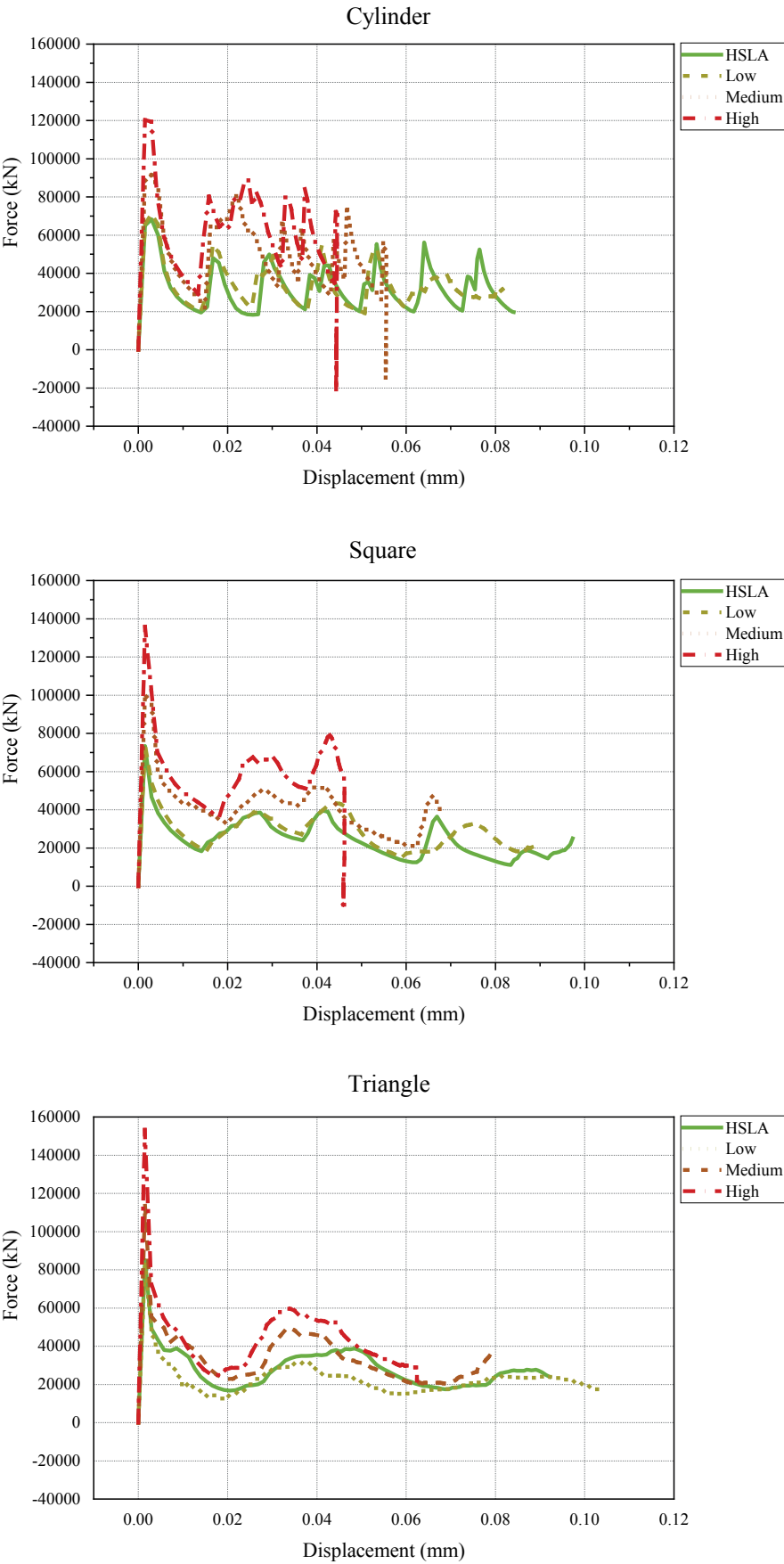
Figure 9 *Force-displacement diagram of finite element simulation results with carbon content and geometry variations*

Table 14 *Finite element simulation output with geometry variations; C = Cylinder, S = Square, and T = Triangle*

	Maximum displacement (mm)			Total energy absorption (J)		
	C	S	T	C	S	T
Temperature	82.07	97.07	89.95	2786.49	2408.41	2597.21
Carbon	66.44	75.41	84.46	2789.31	2646.95	2611.29
Average	74.25	86.24	87.20	2787.90	2527.68	2604.25
	Peak force (kN)			Average force (kN)		
	C	S	T	C	S	T
Temperature	71.64	76.99	89.48	32.74	23.32	27.40
Carbon	87.72	95.82	109.06	34.81	31.62	29.83
Average	79.68	86.40	99.27	33.77	27.47	28.61

and dimensional changes due to temperature changes. Although the various factors affecting the test were taken into account, this study remains an idealistic representation, hence, the results need to be verified with real experiments. However, this study provides important insights into the response of the system to variations in temperature, material composition, and geometry in axial compression tests. To improve the safety and effectiveness of marine transportation in the future, this study is expected to contribute greatly to our understanding of the safety challenges faced by ship structures in harsh environments.

Acknowledgements

Conflicts of interest

The authors declare that they have no known competing financial interests or personal relationships that could have appeared to influence the work reported in this paper.

References

[1] SCHNURR, R. E. J., WALKER, T. R. *Marine transportation and energy use*. In: *Reference Module in Earth Systems and Environmental Sciences*. Amsterdam: Elsevier, 2019. ISBN 9780124095489.

[2] WALKER, T. R. Green marine: an environmental program to establish sustainability in marine transportation. *Marine Pollution Bulletin* [online]. 2016, **105**(1), p. 199-207. ISSN 0025-326X. Available from: https://doi.org/10.1016/j.marpolbul.2016.02.029

[3] LASSERRE, F., PELLETIER, S. Polar super seaways? Maritime transport in the Arctic: an analysis of shipowners' intentions. *Journal Transportation Geography* [online]. 2011, **19**(6), p. 1465-1473. ISSN 0966-6923. Available from: https://doi.org/10.1016/j.jtrangeo.2011.08.006

[4] WALKER, T. R., ADEBAMBO, O., FEIJOO, M. C. D. A., ELHAIMER, E., HOSSAIN, T., EDWARDS, S. J., MORRISON, C. E., ROMO, J., SHARMA, N., TAYLOR, S., ZOMORODI, S. Chapter 27 - Environmental effects of marine transportation [online]. In: *World seas: an environmental evaluation*. Cambridge: SHEPPARD, CH. (Ed.). Academic Press, 2019. ISBN 9780128050521. Available from: https://doi.org/10.1016/B978-0-12-805052-1.00030-9

[5] BRYNOLF, S., LINDGREN, J. F., ANDERSSON, K., WILEWSKA-BIEN, M., BALDI, F., GRANHAG, L., JOHNSON, H., LINNE, P., SVENSSON, E., ZETTERDAHL, M. Improving environmental performance in shipping. In: *Shipping and the environment* [online]. ANDERSSON, K., BRYNOLF, S., LINDGREN, J. F., WILEWSKA-BIEN, M. (Eds.). 1. ed. Berlin, Heidelberg: Springer, 2016. ISBN 9783662490457. Available from: https://doi.org/10.1007/978-3-662-49045-7

[6] Annual overview of marine casualties and incidents 2017 - European Maritime Safety Agency (EMSA) [online] [accessed 2024-02-07]. Available from: http://emsa.europa.eu/emsa-documents/latest/item/3156-annual-overview-of-marine-casualties-and-incidents-2017.html

[7] CHEN, P., HUANG, Y., MOU, J., van Gelder, P. H. A. J. M. Probabilistic risk analysis for ship-ship collision: State-of-the-art. *Safety Science* [online]. 2019, **117**, p. 108-122. ISSN 0925-7535. Available from: https://doi.org/10.1016/j.ssci.2019.04.014

[8] HUANG, Y. CHEN, L., CHEN, P., NEGENBORN, R. R., VAN GELDER, P. H. A. J. M. Ship collision avoidance methods: state-of-the-art. *Safety Science* [online]. 2020, **121**, p. 451-473. ISSN 0925-7535. Available from: https://doi.org/10.1016/j.ssci.2019.09.018

[9] PRABOWO, A. R., RIDWAN, R., TUSWAN, T., SMARADHANA, D.F., CAO, B., BAEK, S. J. Crushing resistance on the metal-based plate under impact loading: a systematic study on the indenter radius influence in grounding accident. *Applications in Engineering Science* [online]. 2024, **18**(4), 100177. ISSN 2666-4968. Available from: https://doi.org/10.1016/j.apples.2024.100177

[10] FAQIH, I., ADIPUTRA, R., PRABOWO, A. R., MUHAYAT, N., EHLERS, S., BRAUN, M. Hull girder ultimate strength of bulk carrier (HGUS-BC) evaluation: structural performances subjected to true inclination conditions of stiffened panel members. *Results in Engineering* [online]. 2023, **18**, 101076. ISSN 2590-1230. Available from: https://doi.org/10.1016/j.rineng.2023.101076

[11] LUTFI, Y. M., ADIPUTRA, R., PRABOWO, A. R., UTSUNOMIYA, T., ERWANDI, E., MUHAYAT, N. Assessment of the stiffened panel performance in the OTEC seawater tank design: parametric study and sensitivity analysis. *Theoretical Application Mechanics Letters* [online]. 2023, **13**(4), 100452. ISSN 2095-0349. Available from: https://doi.org/10.1016/j.taml.2023.100452

[12] Annual overview of marine casualties and incidents 2023 - European Maritime Safety Agency (EMSA) [online] [accessed 2024-05-05]. Available from: https://www.emsa.europa.eu/component/flexicontent/download/7639/5055/23.html

[13] XU, M. C., SONG, Z. J., ZHANG, B. W., PAN, J. Empirical formula for predicting ultimate strength of stiffened panel of ship structure under combined longitudinal compression and lateral loads. *Ocean Engineering* [online]. 2018, **162**, p. 161-175. ISSN 0029-8018. https://doi.org/10.1016/j.oceaneng.2018.05.015

[14] HABIB, M. I., ADIPUTRA, R., PRABOWO, A. R., ERWANDI, E., MUHAYAT, N., YASUNAGA, T., EHLERS, S., BRAUN, M. Internal flow effects in OTEC cold water pipe: finite element modelling in frequency and time domain approaches. *Ocean Engineering* [online]. 2023, **288**(1), 116056. ISSN 0029-8018. Available from: https://doi.org/10.1016/j.oceaneng.2023.116056

[15] HANIF, M. I., ADIPUTRA, R., PRABOWO, A. R., YAMADA, Y., FIRDAUS, N. Assessment of the ultimate strength of stiffened panels of ships considering uncertainties in geometrical aspects: finite element approach and simplified formula. *Ocean Engineering* [online]. 2023, **286**(1), 115522. ISSN 0029-801. Available from: https://doi.org/10.1016/j.oceaneng.2023.115522

[16] HUHNE, C., ROFLES, R., BREITBACH, E., TESSMER, J. Robust design of composite cylindrical shells under axial compression - simulation and validation. *Thin-Walled Structure* [online]. 2008, **46**(7-9), p. 947-962. ISSN 0263-8231. Available from: https://doi.org/10.1016/j.tws.2008.01.043

[17] MCGREGOR, C. J., VAZIRI, R., POURSARTIP, A., XIAO, X. Simulation of progressive damage development in braided composite tubes under axial compression. *Composite Part A: Application Science and Manufacturing* [online]. 2007, **38**(11), p. 2247-2259. ISSN 1359-835X. Available from: https://doi.org/10.1016/j.compositesa.2006.10.007

[18] GREINER, R., KETTLER, M. Interaction of bending and axial compression of stainless steel members. *Journal of Construction Steel Research* [online]. 2008, **64**(11), p. 1217-1224. ISSN 0143-974X. Available from: https://doi.org/10.1016/j.jcsr.2008.05.008

[19] PAIK, J. K., LEE, D. H., NOH, S. H., PARK, D. K., RINGSBERG, J. W. Full-scale collapse testing of a steel stiffened plate structure under axial-compressive loading triggered by brittle fracture at cryogenic condition. *Ships and Offshore Structures* [online]. 2020, **15**(sup1), p. S29-S45 ISSN 1744-5302. Available from: https://doi.org/10.1080/17445302.2020.1787930

[20] SCHOYEN, H., BRATHEN, S. The northern sea route versus the Suez Canal: cases from bulk shipping. *Journal of Transportation Geography* [online]. 2011, **19**(4), p. 977-983 [accessed 2024-02-12]. ISSN 0966-6923. Available from: https://doi.org/10.1016/j.jtrangeo.2011.03.003

[21] KITAGAWA, H. Arctic routing: challenges and opportunities. *WMU Journal of Maritime Affairs* [online]. 2008, **7**(2), p. 485-503 ISSN 1651-436X. Available from: https://doi.org/10.1007/BF03195147

[22] Arctic marine shipping assessment 2009 report - Protection of Arctic Marine Environment (PAME) [online] [accessed 2024-02-14]. Available from: https://www.pmel.noaa.gov/arctic-zone/detect/documents/AMSA_2009_Report_2nd_print.pdf

[23] BAKSH, A. A., ABBASSI, R., GARANIYA, V., KHAN, F. Marine transportation risk assessment using Bayesian Network: application to Arctic waters. *Ocean Engineering* [online]. 2018, **159**, p. 422-436. ISSN 0029-8018. Available from: https://doi.org/10.1016/j.oceaneng.2018.04.024

[24] PRATAMA, A. A., PRABOWO, A. R., MUTTAQIE, T., MUHAYAT, N., RIDWAN, R., CAO, B., LAKSONO, F. B. Hollow tube structures subjected to compressive loading: implementation of the pitting corrosion effect in nonlinear FE analysis. *Journal of the Brazilian Society of Mechanical Sciences and Engineering* [online]. 2023, **45**(3), 143. ISSN 1678-5878. Available from: https://doi.org/10.1007/s40430-023-04067-3

[25] JOHNSON, G. R., COOK, W. H. Fracture characteristics of three metals subjected to various strains, strain rates, temperatures and pressures. *Engineering Fracture Mechanics* [online]. 1985, **21**(1), p. 31-48. ISSN 0013-7944. Available from: https://doi.org/10.1016/0013-7944(85)90052-9

[26] SINGH, R. *Applied welding engineering*. Oxford: Butterworth-Heinemann, 2020. ISBN 9780123919175.

[27] UTAMI, N. P. E., ELLYANIE, E., NASUTION, J. D. The effect of lead (Pb) hot dipping on seawater corrosion rate in ASTM A36 steel. *IOP Conference Series: Materials Science and Engineering* [online]. 2019, **620**, 012108. ISSN 1757-899X. Available from: https://doi.org/10.1088/1757-899X/620/1/012108

[28] SENTHILKUMAR, N., TAMIZHARASAN, T. Effect of tool geometry in turning AISI 1045 steel: experimental investigation and FEM analysis. *Arabian Journal for Science and Engineering* [online]. 2014, **39**(6), p. 4963-4975. ISSN 2191-4281. Available from: https://doi.org/10.1007/s13369-014-1054-2

[29] HUSSAIN, A., PODGURSKY, V., GOLJANDIN, D., ANTONOV, M., BASIT, M. A., AHMAD, T. Mild steel tribology for circular economy of textile industries. *Tribology in Industry* [online]. 2021, **43**(4), p. 552-560. ISSN 0354-8996. Available from: http://dx.doi.org/10.24874/ti.1050.02.21.04

[30] ZHOU, C. YE, Q., YAN, L. Effect of ultra and fast cooling on microstructure and properties of high strength steel for shipbuilding [online]. In: *HSLA steels 2015, microalloying 2015 and offshore engineering steels 2015*. The Chinese Society for Metals (CSM), Chinese Academy of Engineering (CAE) (Eds.). Cham: Springer, 2015. ISBN 978-3-319-48614-7. Available from: https://doi.org/10.1007/978-3-319-48767-0_147

[31] AGARANA, M. C., AKINLABI, E. T. Modelling of A36 steel plate dynamic response to uniform partially distributed moving iron load using differential transform method. *IOP Conference Series: Materials Science and Engineering* [online]. 2018, **413**, 012011. ISSN 1757-899X. Available from: https://doi.org/10.1088/1757-899X/413/1/012011

[32] ELSHENAWY, T., LI, Q. M. Influences of target strength and confinement on the penetration depth of an oil well perforator. *International Journal of Impact Engineering* [online]. 2013, **54**, p. 130-137 [accessed 2024-02-16]. ISSN 0734-743X. Available from: https://doi.org/10.1016/j.ijimpeng.2012.10.010

[33] SEIDT, J. D., GILAT, A., KLEIN, J. A., LEACH, J. R. High strain rate, high temperature constitutive and failure models for EOD impact scenarios. In: SEM Annual Conference and Exposition on Experimental and Applied Mechanics: proceedings. 2007. ISBN 9781604232226.

[34] HAN, G., LEE, K. M., KIM, S. K. A study on improving dynamic characteristics of a front lower suspension arm and aerodynamic effects of a hand-made hybrid vehicle. *International Journal of Precision Engineering and Manufacturing* [online]. 2014, **15**(9), p. 1897-1908. Available from: https://doi.org/10.1007/s12541-014-0544-1

[35] CHEN, W., HUO, D., TENG, X., SUN, Y. Surface generation modelling for micro end milling considering the minimum chip thickness and tool runout. *Procedia CIRP* [online]. 2017, **58**, p. 364-369. ISSN 2212-8271. Available from: https://doi.org/10.1016/j.procir.2017.03.237

[36] DONG, Y., REN., Y., FAN, S., WANG, Y., ZHAO, S. Investigation of notch-induced precise splitting of different bar materials under high-speed load. *Materials* [online]. 2020, **13**(11), 2461. eISSN 1996-1944. Available from: https://doi.org/10.3390/ma13112461

[37] TAK, S. K., IQBAL, M. A. Axial compression behaviour of thin-walled metallic tubes under quasi-static and dynamic loading. *Thin-Walled Structures* [online]. 2021, **159**, 107261. ISSN 0263-8231. Available from: https://doi.org/10.1016/j.tws.2020.107261

[38] HARIS, S., AMDAHL, J. Analysis of ship-ship collision damage accounting for bow and side deformation interaction. *Marine Structures* [online]. 2013, **32**, p. 18-48. ISSN 0951-8339. Available from: https://doi.org/10.1016/j.marstruc.2013.02.002

[39] SURYANTO, S., PRABOWO, A. R., MUTTAQIE, T., ISTANTO, I., ADIPUTRA, R., MUHAYAT, N., FAJRI, A., BRAUN, M., EHLERS, S. Evaluation of high-tensile steel using nonlinear analysis: experiment-FE materials benchmarking of LNG carrier structures under low-temperature conditions. *Energy Reports* [online]. 2023, **9**(9), p. 149-161. ISSN 2352-4847. Available from: https://doi.org/10.1016/j.egyr.2023.05.252